MAIN RING MAGNET SYSTEM OF KEK PS

A. Ando, K. Endo, T. Kasuga, M. Kihara and E. Takasaki
National Laboratory for High Energy Physics
Oho-machi, Ibaraki, Japan

Summary

Results of the field measurement on the quadrupole and bending magnets for the main ring of KEK 12 GeV proton accelerator are shown. The design of secondary magnets is reported.

Introduction

The main ring of the KEK 12 GeV proton accelerator is the separated function synchrotron with the four long straight sections[1]. There are 48 bending magnets and 56 quadrupole magnets in the ring, and two quadrupole magnets and one bending magnet, which serve as the reference magnets for the main ring B-clock system, are set up in the power house.

All magnets have already been set into the tunnel by March and the precise alignment is now going on. The magnetic field measurement on the quadrupole magnet was performed before installed into the tunnel. On the bending magnet, however, the field measurement is in progress inside the main ring tunnel.

The design of the secondary magnets has already finished. The following secondary magnets are installed in the main ring; the horizontal and vertical steering magnets, the trimming quadrupole magnets, the skew quadrupole magnets, the sextupole magnets, and the octupole magnets.

The steering magnets are always used in dc excitation. The other correction magnets are also energized by dc power supplies in the initial operation of the main ring, so as to provide correction only at injection, although magnets themselves are designed to permit future pulsed operation with the full excitation at the maximum energy. All magnets are excited by individual power supplies to generate harmonics with changeable amplitude and phase.

In this report, the results of the field measurements on the quadrupole and bending magnets, and the design of the secondary magnets are given.

Magnetic Field Measurements

Quadrupole magnet

Magnetic field measurements were performed on 60 quadrupole magnets before installed in the main ring tunnel. As the basic measurements on each magnet, the excitation curve of the field gradient, the transversal distributions of the field gradient at the center of magnet and the effective gradient length $(1/B')\int B'ds$ on the magnet axis were measured at eight excitation levels from 0.13 kG/cm to 2.04 kG/cm.

These field measurements were done under the dynamic operation by using two digital integrators connected with the conventional twin coils and the reference coil. The long coil 10 cm long was used for measurements of the effective gradient length. In order to check the stability of the measuring system, one particular magnet was chosen as the standard magnet, on which the above-mentioned quantities were frequently measured. The results of this measurement have shown the rms statistical error to be less than 0.02 % for both the field gradient and the effective gradient length at all excitation levels.

The remanent field was also measured by the Hall generator after exciting the magnet up to 2.0 kG/cm. The relative error for the remanent field gradient is less than 4 %, and the accuracy in its absolute value is estimated to be at most 7 %.

The radial distributions of the effective gradient length on the standard magnet are shown in Fig.1. As the result of the multipole expansion, the effective gradient length contains the 12th multipole as the main higher component, rather than the octupole as shown in Table 1. It is the particular feature of using the oriented steel that the higher multipole components in the effective length do not change appreciably with the field strength.

The histograms of the field gradient, the effective gradient length and the integral of field gradient $\int B'ds$ are shown in Fig.2. The average value and the standard deviation for these quantities are given in Table 2. The fluctuation in $\int B'ds$, which is the most interesting quantity from the viewpoint of the operation of the machine, is less than 8×10^{-4} at all excitation levels.

The average value of the remanent field gradient is 0.58 G/cm with the fluctuation of 0.04 G/cm. This fluctuation corresponds to 3×10^{-4} at injection field of 150 G/cm. In Table 2, the effect of the remanent field is added to the field gradient produced by the exciting current, for B' = 0.128 kG/cm.

Bending magnet

Magnetic measurements on the 48 bending magnets have not yet been finished. In this section, the measured results on one bending magnet are reported.

The bending magnet is measured under the dynamic operation by using the same measuring system as that for the quadrupole magnet. The remanent field is also measured by the Hall generator after pulsing the magnet up to 17.5 kG.

As reported in the previous paper[2], a slight amount of gradient exists in the field produced by the exciting current. The k-value at the injection field is $-0.017\ m^{-1}$ and it decreases with increasing field strength to reach an almost constant value of $-0.005\ m^{-1}$ above a certain field level. This variation of the field gradient may be attributed to the systematic gap opening during welding, the gap deformation due to the magnetic force and the core saturation.

The remanent field on the magnet centerline is 6.6 G and the gradient is 12 G/m. This can be partly cancelled by the field gradient produced by the exciting current (i.e. B' = -25.5 G/m at the injection field).

The radial distribution of the effective length was measured at 1.5, 7.5, 12.2 and 15.8 kG along the coordinate system shown in Fig.3. At low fields, the integral of the field strength over the central part of magnet is little dependent on the radial position. Therefore, the multipole components included in the effective length are mainly governed by the contribution from the fringing field at both ends. Above the medium fields, however, the field integral over the central part of the magnet is dependent on the position. The multipole components included in the effective length are listed in Table 3.

Although the power supply capability limited the maximum excitation to 15.8 kG for full scale magnet, we have roughly estimated the effective length from the data of the half-length magnet. The effective length for the half-length magnet is 1614.9 mm and the sextupole coefficient a_2/a_0 is $-1.2\ m^{-2}$. Considering that the sextupole component of the field strength at the magnet center is $-1.1\ m^{-2}$, the sextupole component included in the effective length for the full scale magnet can be approximated to be $a_2/a_0 = -1.13\ m^{-2}$.

Design of Secondary Magnets

The secondary magnets consist of 56 steering magnets, 16 trimming quadrupole magnets, 8 skew quadrupole magnets, 8 sextupole magnets and 16 octupole magnets. They are installed in the midi straight sections after F and D quadrupole magnet, in such a manner that they have the same superperiodicity as the main lattice.

Although strict tolerances were imposed on the main magnets, the variation in field strength and the misalignment of magnets yield the closed orbit distortion, which is estimated to be 13 mm in the horizontal plane and 6 mm in the vertical plane. Also, the variation in the field gradient and the field imperfections caused by the fringing field and the saturation effect excite the linear and non-linear resonances.

In Table 4 are summarized the principal parameters of the secondary magnets, and the proposed location for these magnets is shown in Fig.4. The secondary magnets are energized by dc power supplies, in the initial operation of the accelerator, to provide the correction only at injection. However, these magnets except for the steering magnet are made of laminated cores to permit future pulsed operation.

Steering magnet and closed orbit correction

The closed orbit distortion is caused by misalignment and random variation in field strength of the main magnets. The correction is done by the steering magnets at injection, and the displacement of the main quadrupole magnets at high fields.

The steering magnets are placed after every quadrupole magnet; 28 horizontal steering magnets follow the main F quadrupoles and 28 vertical ones the main D quadrupoles. The position of the closed orbit is measured with 56 beam position monitors which are fixed at the downstream end of every main quadrupole magnet. The field strength of the steering magnets listed in Table 4 is sufficient for providing the local closed orbit bump less than the half-aperture in both planes.

Current of the steering magnets is adjusted with a method based on the least squares theory.[3] The correcting deflections represented by a vector $\vec{\theta}$ are related to the measured distortion $\vec{x}$ in the following form;

$$\vec{x} + A\vec{\theta} = 0 , \qquad (1)$$

where A is a matrix constructed from the betatron oscillation variables. Since the solution of the above equation suffers from sensor error, besides A has no inverse matrix, it is relevant to treat eq.(1) as the least square problem in which the norm $||\vec{x} + A\vec{\theta}||^2$ is minimized. After simple manipulations, we get

$$\vec{B} + M\vec{\theta} = 0 ,$$

where $\vec{B} = A^T \vec{x}$ and $M = A^T A$. The matrix M is symmetric and has real and non-negative eigenvalues. The eigenvectors with low eigenvalue give only minor effects on the closed orbit and can be deleted from the solution.[3]

In Fig.5 the eigenvalues are arranged in order of their dominant frequency, showing a resonant sensitivity to distortions with frequency near the ν value.

Fig.6 shows examples of closed orbit correction, assuming that the original closed orbit has the distorted sinusoidal form with frequency of 7.25. The effect of monitor failure has been studied by letting the distortion at the failed monitor be zero. In order to reduce the maximum closed orbit distortion by a factor of 2 or 3, it is sufficient to select 10 eigenvectors even in the presence of 3 failed monitors.

The closed orbit correction at high fields is performed in the similar way by replacing the deflection $\vec{\theta}$ by the displacement of the main quadrupole magnets and constructing a new matrix A.[4]

The power supplies for the steering magnets will permit independent control of individual current. A block diagram for this system is shown in Fig.7. Information such as magnet location and current is transmitted to each power supply in the digital form through transmission lines. Each magnet current is changed after converting the digital settings into an analogue value.

Trimming quadrupole magnet

The trim quadrupole magnets are used for independent tuning of the horizontal and vertical betatron frequencies and exciting the 15th harmonic to cancel the stopband of the half integer resonance at $\nu = 7.5$.[5] The error quadrupole field comes from the variations in the gradient length $\int B'ds$ of the quadrupole magnet and the k-value in the bending magnet.

Correcting sextupole and octupole magnets may be the source of gradient error when the excursion of closed orbit from the center of magnets is present. Similarly, the higher multipole components in the bending magnet yield the same effect.

In the "fine tuning" mode, the trim quadrupole should not excite any harmonics in the neighbourhood of $2\nu_x$ and $2\nu_z$, such as 14th, 15th and 16th. As the trim quadrupoles have the same periodicity as the main lattice, the harmonics of multiple of 4 are excited. To eliminate the 16th harmonic, the current of the quadrupoles in one superperiod must be properly modulated. Although the complete elimination is impossible with 4 quadrupoles, the stopband can be suppressed to 0.08 for the tune shift $\Delta\nu = 0.1$, for the proposed arrangement. Since the betatron frequencies can be tuned by the main quadrupoles, the trim quadrupoles are used for fine tuning of $\Delta\nu$ less than 0.2.

The stopband width which is expected from the gradient error in the main magnets is 0.016, assuming the variation of 30 % in the k-value of the bending magnet (Table 5). At 12 GeV, however, the closed orbit excursion (5 mm rms) in the bending magnet produces the stopband width of the same amount. Contribution from the correcting sextupole magnets may be even larger. In the "15th excitation" mode, two quadrupole pairs at the opposite side of the ring are excited with the same gradient but in opposite sign, so as not to excite such harmonics as 0th, 14th and 16th. In order to change the amplitude and phase of the 15th harmonic independently in both planes, eight quadrupoles are used to generate cos and sin functions.

The trim quadrupole magnets are designed to be excited up to 4 T/m, which corresponds to the tune shift $\Delta\nu = 0.1$ for the maximum energy. At first, however, the trim quadrupoles are excited by dc power supplies up to 0.7 T/m which will provide the tune shift $\Delta\nu = 0.2$ at

the injection field. The required strength for the 15th harmonic excitation is smaller than this, so that both modes are easily superimposed.

Skew quadrupole magnet

Sources of the skew quadrupole field are the roll of the quadrupole magnets and the vertical closed orbit deviation in the presence of the sextupole field. If an increase of 10 % in emittance due to the coupling oscillation at $\nu_x = \nu_z$ is allowed, the tolerable limit is given by $B'_x = 1.6 \times 10^{-5}$ T/m at injection and 1.9×10^{-4} T/m at 12 GeV, for $\nu_x - \nu_z = 0.005$. These values correspond to the average roll error of 10^{-5} rad.

The main quadrupole magnets were settled in the tunnel with the roll error less than 10^{-4}. Here, assuming the mean value of roll error to be 5×10^{-5}, the required strength of the skew quadrupole field is obtained as listed in Table 4. Such field is provided by the special windings on the octupole magnet described later.

Sextupole magnet

Sextupole magnets are used for narrowing the stopband of the third order resonance and compensating the chromatic aberration. Source of the sextupole field is mainly the fringing field and the saturation effect in the bending magnet. The sextupole field produced by eddy current in the vacuum chamber is less important in our case because the injection field is high.

The stopband width for each resonance line, which is estimated by using the data of the field measurement, is summarized in Table 5. Here we assumed the roll error of the bending magnet is 10^{-4}rad. As seen in the table, the dangerous resonance is $3\nu_x = 22$ which is near the working point.

The tune shift due to momentum error is $\Delta\nu_x = -0.04$ and $\Delta\nu_z = -0.02$ for $\Delta p/p = 0.3$ % at injection. At 12 GeV, it becomes $\Delta\nu_x = -0.002$ and $\Delta\nu_z = 0$ since $\Delta p/p = 0.1$ %. To compensate this tune shift, especially $\Delta\nu_x$, eight sextupole magnets are used. The required strength is given in Table 4. The field strength required to cancel the 22nd harmonic of sextupole field is smaller than that for compensation of the tune shift.

Octupole magnet

Octupole magnets are used for narrowing the stopband of the fourth order resonance induced by both magnetic imperfections and the space charge force.

The main source of the octupole component is the fringing field and saturation effect of the main quadrupole magnet. Amplitude dependent tune shift due to the octupole field is less than 10^{-3} for the horizontal emittance of $\varepsilon_H = 80\ \pi$ mm-mrad. The stopband width is given in Table 5.

In the presence of momentum spread, the betatron frequency oscillates around a central ν value by virtue of the synchrotron oscillation. When the beam crosses the fourth order resonance lines many times during the acceleration period, the horizontal and vertical emittance growth occurs. Since the growth rate at each traversal of the stopband depends on its width, it should be eliminated by the correcting octupole magnets.

Octupole magnets are also used to provide octupole field with appropriate amplitude and phase for the half integer resonant extraction.

The coupled motion induced by space charge forces drives $2\nu_x - 2\nu_z = 0$ resonance which will result in the emittance blow-up[6]. This can be compensated by the octupole field with the zeroth harmonic. For the intensity of 5×10^{12} protons in the ring, the required strength is 30 G/cm^3 at 12 GeV. This field strength is sufficient for the correction of field error and the half integer resonant extraction.

Acknowledgements

The authors wish to thank Professor T. Nishikawa for many fruitful discussions and continuous support. Thanks are due to Messrs. A. Araki, T. Igarashi and S. Ochiai for preparing the field measurement equipments and carrying out the numerical computation.

References

1. K. Endo and M. Kihara, Proc. 4th Int'l Conf. on Magnet Technology, BNL, 1972, p.363.

2. M. Kihara, Proc. U.S.-Japan Seminar on High Energy Accelerator Science, Tokyo and Tsukuba, 1973, p.134.

3. G.R. Lambertson and L.J. Laslett, Proc. 5th Int'l Conf. on High Energy Accelerators, Frascati, 1965, p.26.

4. G. McD. Bingham, NAL internal report TM-200 (1970).

5. A.G. Ruggiero, NAL internal report TM-348 (1972).

6. B.W. Montague, CERN 68-38 (1968).

7. G. Guignard, CERN 70-24 (1970).

Table 1. Multipole coefficients for the effective gradient length of the quadrupole magnet ($\ell_G = \sum_{n=0}^{14} a_n x^n$)

B' (kG/cm)		0.128	1.777	1.927
a_0	(mm)	615.48	604.15	602.70
a_1/a_0	(m^{-1})	0.029	0.018	0.013
a_2/a_0	(m^{-2})	0.16	-0.21	-0.39
a_3/a_0	(m^{-3})	-11.7	6.1	8.4
a_4/a_0	(m^{-4})	-2040	-2360	-2300
a_5/a_0	(m^{-5})	5100	-20200	-22800

Table 2. Average values and standard deviations of $\frac{dB}{dx}$, L_G and $\int\frac{dB}{dx}ds$ for the quadrupole magnet

$\frac{dB}{dx}$ (kG/cm)	$\sigma(\frac{dB}{dx})$ (%)	L_G (mm)	$\sigma(L_G)$ (%)	$\int\frac{dB}{dx}ds$ (kG)	$\sigma(\int\frac{dB}{dx}ds)$ (%)
0.128	0.047	615.66	0.050	7.832	0.059
1.268	0.058	610.65	0.055	77.40	0.075
1.777	0.058	603.76	0.076	107.26	0.079
1.927	0.050	602.24	0.088	116.02	0.047

Table 3. Multipole coefficients for the effective length of the bending magnet

$$(\ell_B = \sum_{n=0}^{5} a_n x^n)$$

B	(kG)	1.5	7.5	12.2	15.8
a_0	(mm)	3257.0	3254.4	3243.7	3228.8
a_1/a_0	(m^{-1})	-0.0067	-0.0037	-0.0043	0.002
a_2/a_0	(m^{-2})	-0.24	-0.18	-0.24	-0.47

Note that, as seen in Fig.3, the fluctuation in measured values at 1.5 kG is somewhat larger.

Table 4. Principal parameters of the secondary magnets

	Number	Length (m)	Field strength at injection	Field strength at 12 GeV	Power supply
Steering magnet					
horizontal	28	0.15	920 G	-	dc
vertical	28	0.15	370 G	-	dc
Trim quadrupole	16	0.15	70 G/cm	0.4 kG/cm	pulsed
Skew quadrupole	8	0.2	9 G/cm	100 G/cm	pulsed
Sextupole magnet	8	0.4	8 G/cm^2	190 G/cm^2	pulsed
Octupole magnet	16	0.2	0.25 G/cm^3	30 G/cm^3	pulsed

Table 5. Total stopband width

N	n_1	n_2	injection	12 GeV		
2	2	0	0.016	0.008	$\langle\Delta B'/B'\rangle = 8\times10^{-4}$ for QM	
	1	1	1.8×10^{-6}	5.7×10^{-7}	$\langle\Delta B'\rangle$ = 8 G/m (inj)	} for BM
	0	2	0.016	0.008	30 G/m (12 GeV)	
3	3	0	0.027	0.039	B'' = 0.07 T/m^2 (inj)	} for BM
	2	1	3.3×10^{-6}	4.6×10^{-6}	4 T/m^2 (12 GeV)	
	1	2	0.033	0.046		
	0	3	1.2×10^{-6}	1.7×10^{-6}		
4	4	0	1.4×10^{-3}	1.5×10^{-4}	B''' = 0.6 T/m^3 (inj)	} for QM
	3	1	4.7×10^{-8}	4.4×10^{-9}	8 T/m^3 (12 GeV)	
	2	2	6.3×10^{-4}	5.7×10^{-5}		
	1	3	3.3×10^{-8}	3.1×10^{-9}		
	0	4	3.3×10^{-4}	3.3×10^{-5}		

Roll error is assumed to be 5×10^{-5}rad and 10^{-5}rad for QM and BM. < > means rms error.

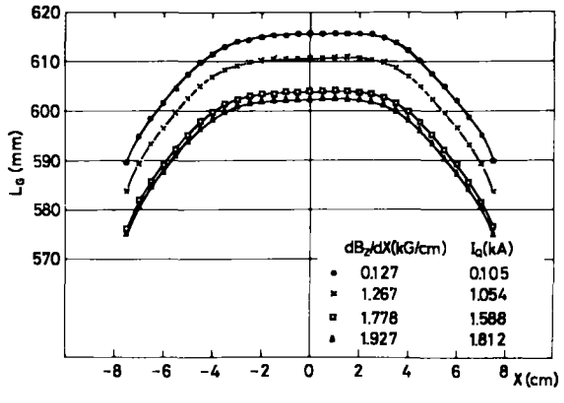

Fig.1 Radial distributions of the effective gradient length of the quadrupole magnet.

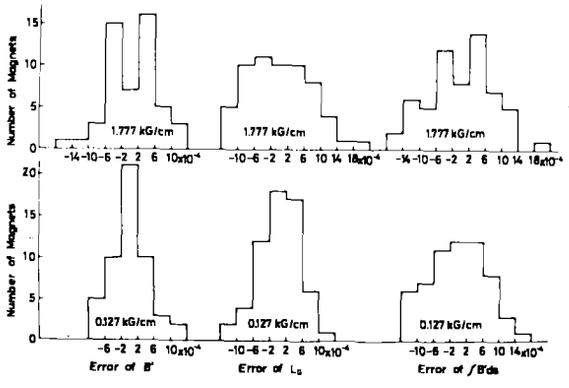

Fig.2 Deviations in $\frac{dB}{dx}$, L_G and $\int\frac{dB}{dx}ds$ of the quadrupole magnet.

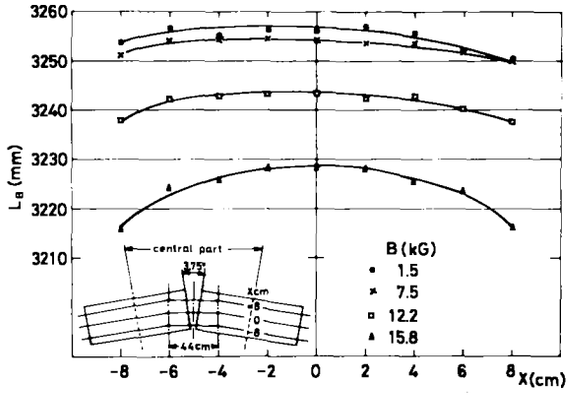

Fig.3 Radial distributions of the effective length of the bending magnet.

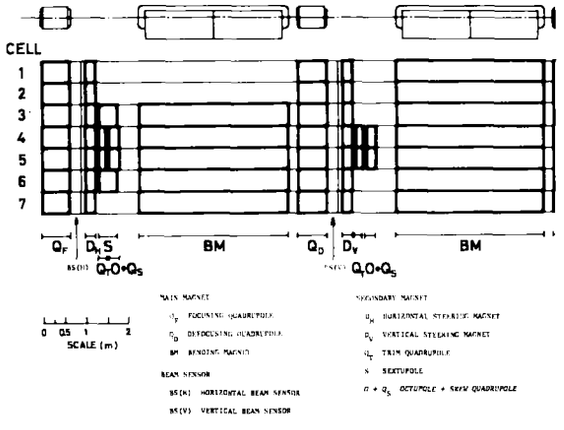

Fig.4 Secondary magnet locations.

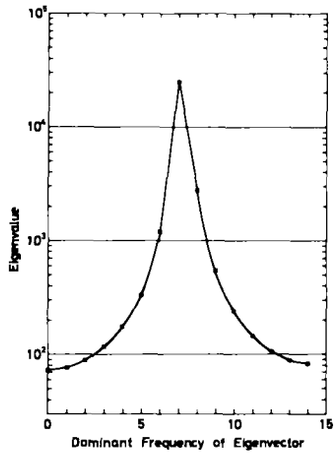

Fig.5 Eigenvalues arranged in order of dominant frequency of eigenvectors. They are doubly degenerated except for both ends.

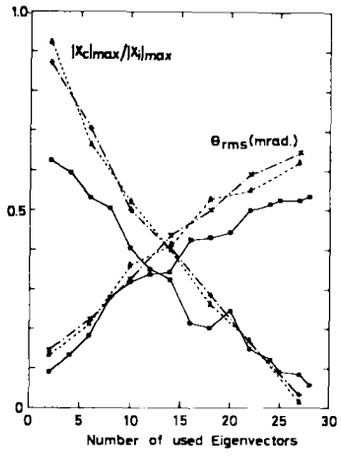

Fig.6 Ratio of the maximum orbit distortion after and before correction, and rms value of correcting deflections as the function of number of used eigenvectors. Solid lines: no monitor failure. Dotted lines: three monitors in failure. Dash-dotted lines: three consecutive monitors in failure.

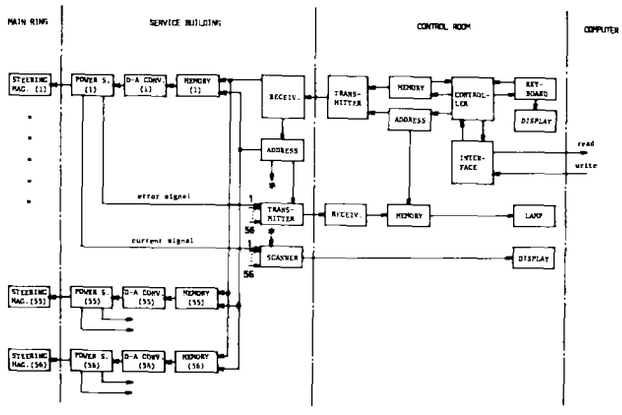

Fig.7 Block diagram of the control system for the steering magnet power supply.